

Excellent thermoelectric performance predicted in Sb_2Te with natural superlattice structure

Pei Zhang(张培), Tao Ouyang(欧阳滔), Chao Tang(唐超), Chaoyu He(何朝宇), Jin Li(李金), Chunxiao Zhang(张春小), and Jianxin Zhong(钟建新)

Citation: Chin. Phys. B, 2021, 30 (**12**): 128401. DOI: 10.1088/1674-1056/ac012c
Journal homepage: http://cpb.iphy.ac.cn; http://iopscience.iop.org/cpb

What follows is a list of articles you may be interested in

Thermoelectric properties of orthorhombic silicon allotrope Si (oP32) from first-principles calculations

Pei Zhang(张培), Tao Ouyang(欧阳滔), Chao Tang(唐超), Chao-Yu He(何朝宇), Jin Li(李金), Chun-Xiao Zhang(张春小), and Jian-Xin Zhong(钟建新)
Chin. Phys. B, 2020, 29 (**11**): 118401. DOI: 10.1088/1674-1056/aba2e1

Fundamental and progress of Bi_2Te_3-based thermoelectric materials

Min Hong(洪敏), Zhi-Gang Chen(陈志刚), Jin Zou(邹进)
Chin. Phys. B, 2018, 27 (**4**): 048403. DOI: 10.1088/1674-1056/27/4/048403

Graphene-enhanced thermoelectric properties of p-type skutterudites

Dandan Qin(秦丹丹), Yuan Liu(刘媛), Xianfu Meng(孟宪福), Bo Cui(崔博), Yaya Qi(祁亚亚), Wei Cai(蔡伟), Jiehe Sui(隋解和)
Chin. Phys. B, 2018, 27 (**4**): 048402. DOI: 10.1088/1674-1056/27/4/048402

Enhancement of thermoelectric properties of $SrTiO_3$/LaNb-$SrTiO_3$ composite by different doping levels

Ke-Xian Wang(王柯鲜), Jun Wang(王俊), Yan Li(李艳), Tao Zou(邹涛), Xiao-Huan Wang(王晓欢), Jian-Bo Li(李建波), Zheng Cao(曹正), Wen-Jing Shi(师文静), Xinba Yaer(新巴雅尔)
Chin. Phys. B, 2018, 27 (**4**): 048401. DOI: 10.1088/1674-1056/27/4/048401

Charge and spin-dependent thermal efficiency of polythiophene molecular junction in presence of dephasing

Z. Golsanamlou, M. Bagheri Tagani, H. Rahimpour Soleimani
Chin. Phys. B, 2015, 24 (**10**): 108402. DOI: 10.1088/1674-1056/24/10/108402

Excellent thermoelectric performance predicted in Sb_2Te with natural superlattice structure*

Pei Zhang(张培), Tao Ouyang(欧阳滔)†, Chao Tang(唐超), Chaoyu He(何朝宇), Jin Li(李金), Chunxiao Zhang(张春小), and Jianxin Zhong(钟建新)‡

Hunan Key Laboratory for Micro-Nano Energy Materials & Device and School of Physics and Optoelectronics, Xiangtan University, Xiangtan 411105, *China*

(Received 2 March 2021; revised manuscript received 30 April 2021; accepted manuscript online 14 May 2021)

Using first-principles calculations combined with the Boltzmann transport theory, we explore the thermoelectric properties of natural superlattice (SL) structure Sb_2Te. The results show that n-type Sb_2Te possesses larger Seebeck coefficient of 249.59 (318.87) μV/K than p-type Sb_2Te of 219.85 (210.38) μV/K and low lattice thermal conductivity of 1.25 (0.21) W/mK along the in-plane (out-of-plane) direction at 300 K. The excellent electron transport performance is mainly attributed to steeper density of state around the bottom of conduction band. The ultralow lattice thermal conductivity of Sb_2Te is mainly caused by low phonon group velocity and strong anharmonicity. Further analysis shows that the decrease of group velocity comes from flatter dispersion curves which are contributed by the Brillouin-zone folding. The strong anharmonicity is mainly due to the presence of lone-pair electrons in Sb_2Te. Combining such a high Seebeck coefficient with the low lattice thermal conductivity, maximum n-type thermoelectric figure of merit (ZT) of 1.46 and 1.38 could be achieved along the in-plane and out-of-plane directions at room temperature, which is higher than the reported values of Sb_2Te_3. The findings presented here provide insight into the transport property of Sb_2Te and highlight potential applications of thermoelectric materials at room temperature.

Keywords: thermoelectric, superlattice (SL), thermal conductivity, phonons

PACS: 84.60.Rb, 73.21.Cd, 65.40.–b, 63.20.–e **DOI:** 10.1088/1674-1056/ac012c

1. Introduction

Thermoelectric (TE) materials can be used in solid-state energy devices that convert waste heat into electricity or electrical power directly into cooling or heating.[1,2] They play an increasingly important role in meeting the present energy challenge due to ubiquitous heat source and pollution free production. Performance of thermoelectric devices is quantified by a dimensionless figure of merit, $ZT = S^2\sigma T/(\kappa_e + \kappa_L)$,[3] which is only related to characteristics of the thermoelectric material and temperature. Here S denotes the Seebeck coefficient, σ is the electrical conductivity, T is the absolute temperature, κ_e and κ_L are the thermal conductivities of electronic and lattice (phononic) contributions, respectively. It is obvious that to obtain a higher ZT value requires a higher Seebeck coefficient, electrical conductivity and lower (electronic and phononic) thermal conductivity. However, coefficients of electronic parts (S, σ and κ_e) always contradict with each other, and it is difficult to increase the numerator and to decrease denominator concurrently, for obtaining a high ZT. Such behavior greatly limits the practical application of thermoelectric technology. Therefore, it has been being a hot spot in the field of thermoelectricity to seek potential materials with high ZT or to improve the thermoelectric conversion efficiency of existing materials.

To date, several strategies have been adopted to enhance the ZT values of TE materials, such as band structure engineering,[4] nanostructuring,[5] phonon-glass electron-crystal,[6] phonon-liquid electron-crystal model,[7] heterostructure formation[8] and quantum confinement effects.[9] In addition to these methods, designing superlattice (SL) structures is also used to improve efficiencies of thermoelectric energy conversion devices.[10] This is because the lattice thermal conductivity can be reduced while the good electron transport performance can be maintained in SL structures.[11,12] Capinski and colleagues[13,14] performed measurements with GaAs/AlAs SLs of various repeat distances. At room temperature, they found that the thermal conductivity of GaAs/AlAs SL is three times to an order of magnitude less than that of bulk GaAs, depending on the repeat distance. Lee *et al.*[15] studied a series of Si/Ge SLs and observed that the thermal conductivities of these samples are lower than those of SiGe alloys. After that, experiment of Venkatasubramanian *et al.* showed that the ZT value of the p-type/n-type SLs consisting of bulk Bi_2Te_3 and Sb_2Te_3 could approach 2.4/1.5 at 300 K.[16,17]

*Project supported by the National Natural Science Foundation of China (Grant Nos. 11974300, 11974299, and 11704319), the Natural Science Foundation of Hunan Province, China (Grant No. 2021JJ30645), the Scientific Research Fund of Hunan Provincial Education Department, China (Grant Nos. 20K127, 20A503, and 20B582), the Program for Changjiang Scholars and Innovative Research Team in Universities (Grant No. IRT13093), and the Hunan Provincial Innovation Foundation for Postgraduate Students, China (Grant No. CX20200624).

†Corresponding author. E-mail: ouyangtao@xtu.edu.cn

‡Corresponding author. E-mail: jxzhong@xtu.edu.cn

© 2021 Chinese Physical Society and IOP Publishing Ltd

Chong *et al.*[18] noted that the lattice thermal conductivity of eight GeTe/Sb_2Te_3 superlattice-like (SLL) layer cycles was less than 30% of that of single layer GeSbTe material. Recently, Tong *et al.*[19] have studied the thermal conductivity of chalcogenide material with an SLL structure, and they pointed out that the thermal conductivity of SLL is lower than those of conventional chalcogenide materials. Very recently, Long *et al.*[20] investigated the phonon properties of phase-change memory (PCM) with an SLL structure. They concluded that the low phonon group velocity and the thermal resistance at interfaces result in the low thermal conductivity of the GeTe/Sb_2Te_3 SLL material. This helped researchers further to understand the physical mechanism of thermal properties in SL structures and to search high-performance TE materials.

Diantimony tellurium (Sb_2Te) is one member in the $(Sb_2)_n$-$(Sb_2Te_3)_m$ infinitely adaptive series, whose crystal structure can be regarded as a natural SL in the *c*-axis direction.[21] This particular structure consists of two Sb_2 bilayers (BLs) interleaved with single quintuple layers (QLs) of Sb_2Te_3.[21,22] In recent years, it was considered as a potential candidate in phase-change memory (PCM) and has been extensively investigated due to the fast crystallization speed of Sb_2Te.[23–26] Previous research mainly concentrated on enhancing the thermal stability of PCM by doping in Sb_2Te.[27,28] However, the study on TE transport for Sb_2Te is still quite scarce until now. Considering the natural advantages of the previously mentioned SL structures, it is interesting and necessary to investigate the thermoelectric transport properties of Sb_2Te, which would be of great significance to explore its potential applications.

In this work, we systematically study the TE transport performance of Sb_2Te using first-principles calculations and Boltzmann transport theory. The calculation results show that the maximum value of ZT of Sb_2Te is as high as 1.46 and 1.38 along the in-plane and out-of-plane directions for n-type doping at 300 K, indicating that such a natural SL material could be a promising material for room temperature TE applications. The rest of this paper is organized as follows. In Section 2, we provide a brief description of the calculation method employed in this work. In Section 3, the results and discussion of electronic, phononic and thermoelectric transport properties are present. Finally, the conclusions of this work are given in Section 4.

2. Method

In this work, the projector augmented wave (PAW) method based on density functional theory (DFT) as implemented in the Vienna *ab initio* simulation package (VASP) was utilized for all the first-principles calculations.[29–31] We used the generalized gradient approximation (GGA) in the Perdew–Burke–Ernzerhof (PBE) as the exchange–correlation functional[32] and van der Waals (vdW) interactions were considered at the vdW-density functional (vdW-DF) level with optB86b-vdW as the exchange functional.[33] The cutoff energy of the plane wave was set as 600 eV and a $16\times16\times3$ Monkhorst–Pack *k*-mesh was employed to sample the Brillouin zone (BZ). The atomic forces were calculated by minimizing the total forces until the energy convergence was less than 10^{-6} eV, while the atomic positions were fully relaxed with Hellman–Feynman force 0.001 eV/A. In order to obtain accurate electronic energy band structure, we adopted Heyd–Scuseria–Ernzerhof (HSE06) screened hybrid functional to calculate the electronic band structure of Sb_2Te.[34,35] Once we obtained the band structure, using the semi-classical Boltzmann transport theory and the rigid band model as implemented in BoltzTrap code,[36] the electronic transport properties could be calculated. Here, we utilized the deformation potential (DP) theory, which is a common method in previous work,[37–41] to evaluate the electronic relaxation time (τ). Within the relaxation time approximation, the Seebeck coefficient and electrical conductivity can be written as[36,42]

$$S(T,E_{\rm F})=-\frac{1}{eTV}\frac{\int\sigma_{\alpha\beta}(E)(E-E_{\rm F})f'(T,E-E_{\rm F})\,{\rm d}E}{\int\sigma_{\alpha\beta}(E)f'(T,E-E_{\rm F})\,{\rm d}E},\quad(1)$$

$$\sigma(T,E_{\rm F})=-\frac{1}{V}\int\sigma_{\alpha\beta}(E)f'(T,E-E_{\rm F})\,{\rm d}E,\quad(2)$$

where $E_{\rm F}$ is relative to the band edge, e is elementary charge, V is the volume of unit cell, f' is the energy derivative of the Fermi function at temperature T, and $\sigma_{\alpha\beta}(E)$ is the energy-dependent transport function defined as

$$\sigma_{\alpha\beta}(E)=e^2\int\nu_\sigma(k)\nu_\beta(k)\tau(k)\delta[E-E(k)]\,{\rm d}^3k,\quad(3)$$

where $E(k)$ is the band energy and $\nu=\nabla_k E/\hbar$ is the group velocity of carriers that can be directly derived from band structures, where $\hbar$ is the reduced Planck constant.

The phonon transport properties of Sb_2Te were obtained by solving the phonon Boltzmann transport equation (PBTE), as implemented in the ShengBTE code with harmonic second-order interatomic force constants ($2^{\rm nd}$ IFCs) and anharmonic third-order IFCs ($3^{\rm rd}$ IFCs) as inputs.[43] The $2^{\rm nd}$ IFCs and phonon dispersion spectrum were calculated using the Phonopy package,[44] and a $3\times3\times1$ supercell with a $3\times3\times2$ *k*-mesh was adopted. The 3rd IFCs, reflecting the properties for the phonon–phonon scattering, were calculated using the same supercell with cutoff of interaction ranging up to sixth nearest neighbors by using Thirdorder.py script.[45] After testing the convergence of the lattice thermal conductivity with respect to the *q*-grid, a dense phonon *q*-grid of $16\times16\times4$ was adopted for Sb_2Te.

3. Results and discussion

Sb_2Te is stacked by Sb_2Te_3 and Sb_2 in the ratio of 1:2 and the layer stacking sequence is –[(Te–Sb–Te–Sb–Te)–(Sb–

Sb)–(Sb–Sb)]–.[21,22] As illustrated in Fig. 1(a), Sb_2Te (space group $P\bar{3}m1$, No. 164) is a hexagonal lattice structure and has 9 atoms in the unit cell. For convenience the hexagonal unit cell with lattice parameters a and c is often used. The lattice constants of Sb_2Te are a $(b) = 4.366$ Å and $c = 17.830$ Å, which are close approximation to previous results ($a = 4.272$ Å and $c = 17.633$ Å).[21,22] As mentioned in the introduction, Sb_2Te can be regarded as a natural SL structure. The electronic band structure and the corresponding density of states (DOS) of Sb_2Te are shown in Figs. 1(b) and 1(c). A local enlargement of the conduction band minimum (CBM) and the valence band maximum (VBM) is also drawn in the illustration in Fig. 1(b). It can be seen that Sb_2Te is a tinny band gap (0.013 eV) semiconductor, which is consistent with the previous work.[21] One can notice that the DOS exhibits abrupt slope near the bottom of conduction bands (CBs). Such a large slope will significantly enhance Seebeck coefficient and electrical conductivity. Meanwhile, multiple conduction band valleys and valence band peaks can be found near the Fermi energy level, which is quite advantageous for the enhancement of ZT and will be discussed in the following.

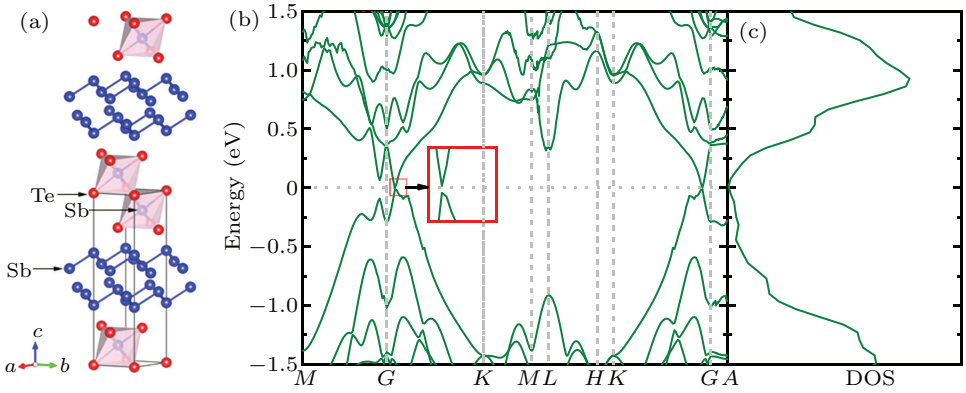


Fig. 1. (a) The crystal structure of Sb_2Te, where Sb and Te atoms are plotted as blue and red spheres, respectively. (b) Electronic band structure and (c) electronic density of states (DOS) of Sb_2Te. The coordinates of the high-symmetry points in the Brillouin zone are M (0, 0.5, 0), Γ (0, 0, 0), K (−0.333, 0.667, 0), L (0.0, 0.5, 0.5), H (−0.333, 0.667, 0.5), K (−0.333, 0.667, 0), A (0, 0, 0.5).

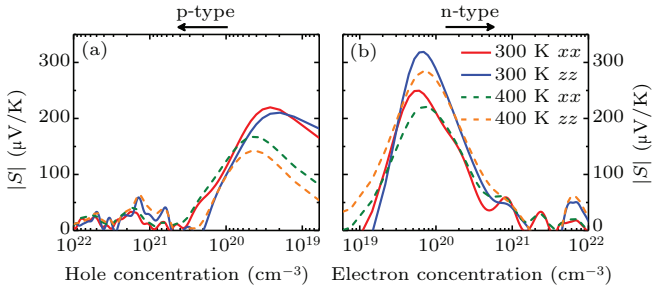


Fig. 2. Seebeck coefficients (absolute value $|S|$) of Sb_2Te as a function of carrier concentration [(a) holes and (b) electrons] along the in-plane (xx) and out-of-plane (zz) directions at 300 and 400 K.

Based on the band structure, the electron transport properties are studied by solving semi-classic Boltzmann transport equation. The rigid band approximation is adopted to simulate the doping effects.[36] The hole and electron concentrations correspond to p- and n-type, respectively. Figures 2(a) and 2(b) show the Seebeck coefficients (S) as a function of carrier concentration at different temperatures along the in-plane (xx) and out-of-plane (zz) directions, respectively. Here, we mainly focus on transport properties around room temperature, thus we only show the relative coefficients at 300 K and 400 K for comparison. According to the Mahan–Sofo theory, S for 3D materials can be written as

$$S = \frac{8\pi^2 k_B T}{3eh^2} m^* \left(\frac{\pi}{3n}\right)^{2/3}, \tag{4}$$

where k_B, h, n, and m^* are the Boltzmann constant, Planck constant, carrier concentration and DOS effective mass around the Fermi energy, respectively. Therefore, there is a competition relation between carrier concentration and effective mass. For low carrier concentration, the Seebeck coefficients (absolute value $|S|$) of Sb_2Te are affected by the bipolar effect in narrow band gap semiconductors and increase with n; while for higher carrier concentration, the calculated S of Sb_2Te is inversely proportional to the n, which is in good agreement with the Mahan-Sofo theory. Interestingly, with the increase of temperature, the peak value of S decreases and moves to the region of higher carrier concentration. Such a phenomenon is mainly related to the excitation of a large number of electrons at higher temperature. Meanwhile, it is also found that $|S|$ for n-type doping is higher than that of the p-type doping, which is caused by steeper DOS around the bottom of CBs. At room temperature, the maximum $|S|$ in p-type doping (at 2.64×10^{19} and 1.96×10^{19} cm^{-3} hole concentration) can reach 219.85 and 210.38 μV/K along the in-plane and out-of-plane directions, respectively. As for n-type doping (at 6.04×10^{19} and 6.91×10^{19} cm^{-3} electron concentrations), the largest Seebeck coefficients are 249.59 and 318.87 μV/K along the in-plane and out-of-plane directions, respectively. Obviously, the Seebeck coefficients of Sb_2Te are much larger than those of Sb_2Te_3 (87 and 72 μV/K along the in-plane direction for p- and n-type doping.[46]) at the same temperature. Such large Seebeck coefficients of Sb_2Te are induced by the multi-valleys

converging effect,[47] which is beneficial for its thermoelectric applications.

Seebeck coefficient is independent of the electron relaxation time (τ), while σ is closely dependent on τ of electrons. The precise treatment of τ depends on the process of detailed scattering mechanism, which is usually very complex. Since the wavelength of thermally activated carriers (electrons or holes) at room temperature is much larger than the lattice constant and is comparable to the wavelength of acoustic phonons, it is widely believed that the scattering of carriers at low energy is dominated by the electron-acoustic phonon coupling, which can be effectively evaluated by the DP theory.[37–41] Using this method, the calculated electron relaxation time of many materials is in good agreement with the experimental data, indicating its accuracy.[48–50] Based on effective mass approximation, the carrier mobility μ for 3D materials can be written in the following form:[38]

$$\mu_{3D} = \frac{2\sqrt{2\pi}e\hbar^4 C_{3D}}{3(k_B T)^{3/2} m^{*5/2} E_1^2}, \tag{5}$$

with $C_{3D} = (\partial^2 E/\partial\delta^2)/V_0$ bing the 3D elastic constant. Here, E is the total energy, δ is the applied strain along the transport direction, and V_0 is the cell volume at equilibrium. $E_1 = \partial E_{edge}/\partial\delta$ is the DP constant, with E_{edge} being the energy of the band edges (VBM for the holes and CBM for the electrons). $M^* = \hbar^2[\partial^2 E(k)/\partial k^2]^{-1}$ is the effective mass along transport direction, with k being the wave-vector magnitude in momentum space. These three quantities can be easily obtained from first-principles calculations. Figure 3(a) shows the relationship between the energy change ($\Delta E = E_\delta - E_{1.0}$, where E_δ is the total energy under strain and $E_{1.0}$ is the original total energy) and lattice dilation along the in-plane and out-of-plane directions, and C_{3D} is obtained by fitting the energy–strain curve. Figures 3(b) and 3(c) describe the shift of both band edges of VBM and CBM as a function of uniaxial strain, where E_1 is calculated from the slope of the fitting lines. Based on the obtained C_{3D}, E_1, and m^*, the carrier mobility and the relaxation time ($\tau = \mu m^*/e$) are calculated as listed in Table 1. Carrier mobility and electron relaxation time show obvious anisotropy due to the anisotropic SL structure of Sb_2Te, which has a significant influence on its electronic properties.

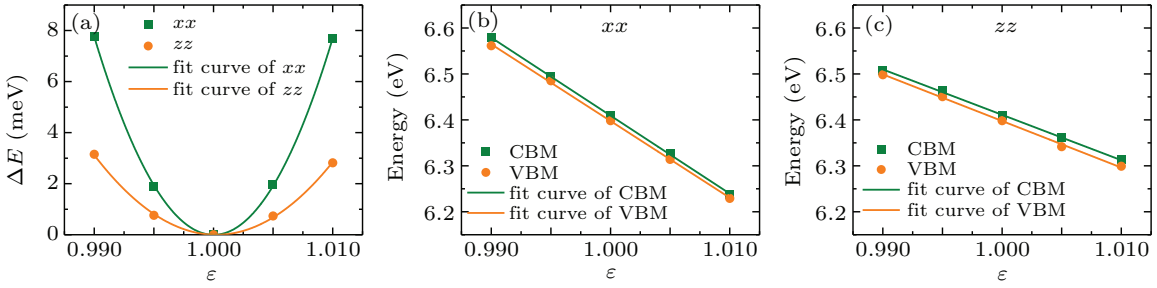


Fig. 3. (a) The relationship between energy change ΔE and lattice dilation along the in-plane (xx) and out-of-plane (zz) directions. (b) and (c) Band energy shifts of VBM and CBM under uniaxial strain along the lattice dilation direction.

Table 1. Deformation potential constants E_1, 3D elastic modulus C_{3D}, effective masses m^*, and carrier mobility μ based on Eq. (2) for in-plane and out-of-plane directions at 300 K.

Carrier type	E_1 (eV)	C_{3D} (eV/A^3)	m^* (m_e)	μ (cm^2·V^{-1}·s^{-1})	τ (s)
Electron (in-plane)	–16.98	0.53	0.40	18.37	4.18×10^{-14}
Hole (in-plane)	–16.71		0.19	122.04	1.32×10^{-13}
Electron (out-of-plane)	–9.88	0.20	0.70	5.17	2.06×10^{-14}
Hole (out-of-plane)	–10.15		1.01	1.96	1.13×10^{-14}

Figures 4(a) and 4(b) present the electrical conductivity σ of Sb_2Te as a function of carrier concentration along the in-plane and out-of-plane directions at 300 and 400 K, respectively. It can be seen that σ monotonously increases with the increasing n in both p- and n-type Sb_2Te. According to the formula $\sigma = ne\mu$, we can realize that σ is proportional to carrier concentration which is contrary to the situation of S as discussed above. Differences of σ along the in-plane and out-of-plane directions can be understood from the carrier mobility as listed in Table 1. With the same carrier concentration, a larger carrier mobility along the in-plane direction results in σ along the in-plane direction being much larger than that along the out-of-plane direction. It is clearly shown that the electrical conductivities of Sb_2Te at 300 and 400 K are comparable when $n < 10^{20}$ cm^{-3}. However, σ at 300 K increases faster than that at 400 K when $n > 10^{20}$ cm^{-3}. This phenomenon can be mainly attributed to the increased electron-phonon scattering with the increasing temperature. In addition, the electrical conductivity of n-type Sb_2Te is larger than that of p-type one, which is similar to the case of S and is also related to the DOS. The electronic thermal conductivity κ_e was estimated by means of Wiedemann–Franz law of $\kappa_e = L\sigma T$, where L is the Lorentz number.[51] As the same as the value in the previous work,[52–54] here we adopt $L = \pi^2\kappa_B^2/3e^2 = 2.44\times10^{-8}$ V^2·K^{-2}. One can note from Figs. 4(c) and 4(d) that the κ_e and σ exhibit analogous curves.

Moreover, the electronic thermal conductivity of Sb_2Te is insensitive to the variation of the temperature. At low carrier concentration ($n < 10^{20}$ cm^{-3}), κ_e is very small and almost negligible. However, κ_e increases with increasing n and negatively affects the ZT of Sb_2Te at high carrier concentration.

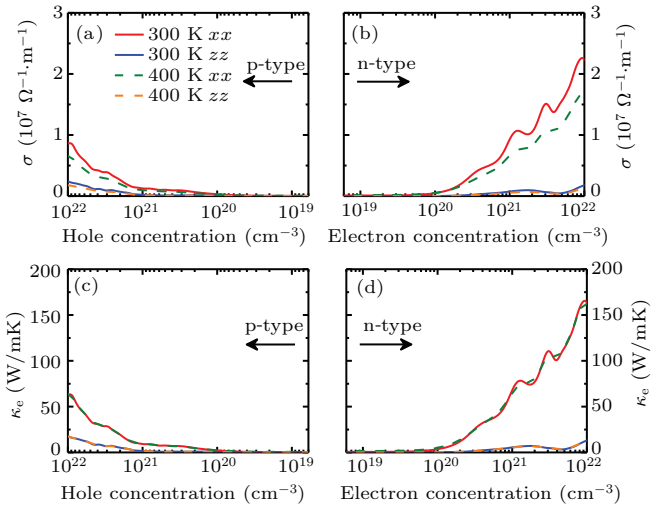


Fig. 4. [(a), (b)] Electrical conductivity σ and [(c), (d)] electronic thermal conductivity κ_e of Sb_2Te versus carrier concentration along the in-plane (xx) and out-of-plane (zz) directions at 300 and 400 K.

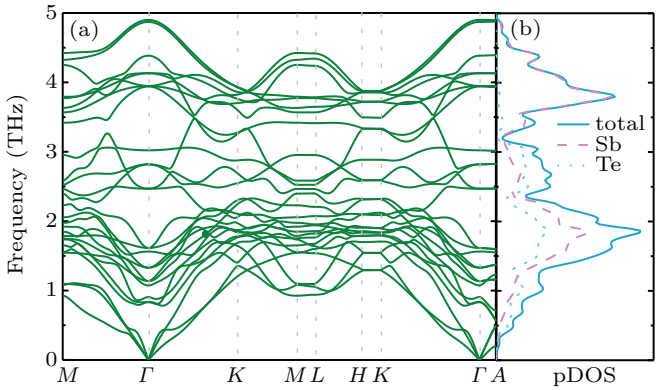


Fig. 5. (a) Calculated phonon dispersion along the high-symmetry paths and (b) the total and partial phonon densities of states (pDOS) for Sb_2Te.

As phonons also play an important role in TE transport, the thermal transport properties of Sb_2Te are explored as well. Figures 5(a) and 5(b) show the phonon dispersion curves, total and partial phonon density of states (pDOS) of Sb_2Te. No negative phonon frequency was observed in Fig. 5(a), indicating the dynamic stability of Sb_2Te. There exist three acoustic and twenty-four optical phonon branches corresponding to the nine atoms in the primitive cell of Sb_2Te. The large masses of Sb and Te atoms induce the phonon dispersion over a smaller frequency scale, and the maximum phonon frequency of Sb_2Te is 4.9 THz. Obviously, there is no phonon band gap between and within the acoustic and optical branches, which means that there is the strong coupling of the acoustic and optical phonon modes. This phenomenon is due to the small difference in atomic masses of the constituent atoms in Sb_2Te, which will lead to the low lattice thermal conductivity. The pDOS contained in Fig. 5(b) illustrates the significant contributions of Sb and Te atoms over the whole frequency range. It is found that the vibrations of Te atomic are mainly on the low frequency (lower than 3.1 THZ) phonon branches while the vibrations of Sb atoms dominate on all the phonon modes.

The lattice thermal conductivity (κ_L) as a function of temperature and q-grid are shown in Fig. 6(a). As plotted in the inset, the phonon thermal conductivity of Sb_2Te achieves good convergence with the increased q-grid. It can be clearly seen that κ_L decreases with increasing temperature, which is a common behavior of 3D materials at medium temperatures.[55–57] In addition, it is worth noting that κ_L along the out-of-plane direction is far smaller than that along the in-plane direction. At room temperature, the lattice thermal conductivities are calculated to be 1.25 and 0.21 W/mK along the in-plane and out-of-plane directions, respectively. Figures 6(b) and 6(c) show the phonon dispersion curves and group velocities of Sb_2Te along Γ–M and Γ–A direction, respectively. The Γ–M and Γ–A directions in the Brillouin zone is equivalent to the in-plane and out-of-plane directions, respectively. One can note that the group velocity of Sb_2Te along the out-of-plane direction is far smaller than that along the in-plane direction, which is one of the reasons for the lower κ_L along the out-of-plane direction than along the in-plane direction. The flatter curve of Sb_2Te along the out-of-plane direction than along the in-plane direction is responsible for this result, because the group velocity is calculated according to $v(q) = \partial\omega(q)/\partial q$, where $\omega(q)$ and q are the phonon frequency and wave vector, respectively. The averaged κ_L can be calculated by $\kappa_L = (\kappa_{xx} + \kappa_{yy} + \kappa_{zz})/3$. Our result for Sb_2Te at 300 K is listed in Table 2, together with available data of Sb_2Te_3 for comparison.[58–61] Interestingly, the averaged κ_L of Sb_2Te is 0.9 W/mK, which is much lower than that reported for bulk Sb_2Te_3, e.g., 4.1 W/mK.[59] As mentioned earlier, Sb_2Te can be regarded as a natural SL in the c-axis direction, thus we take out-of-plane direction as an example to further understand the ultralow $\kappa_L$of Sb_2Te. The phonon dispersion curves and group velocities of Sb_2Te_3 is also depicted in Figs. 6(b) and 6(c) for comparison. Obviously, group velocities of Sb_2Te are lower than that of Sb_2Te_3 along the same direction. The significantly low group velocity could come from the increasing probability of the interface scattering in the SL structure, which acts as the obstacles for the transport of phonons.[62,63] Meanwhile, the flattening of the dispersion curves associated with Brillouin-zone folding also has an effect on the low group velocity.[64] The phonon relaxation time is another vital parameter to determine lattice thermal conductivity. As shown in the inset of Fig. 6(c), the phonon relaxation time for Sb_2Te is between 0.1 and 100 ps. Such low phonon relaxation time implies that there is strong anharmonic phonon scattering. The Grüneisen parameter (γ)

can be used to analyze the anharmonic properties of material, which can be calculated by

$$\gamma(q) = -\frac{V}{\omega(q)}\frac{\partial\omega(q)}{\partial V}, \tag{6}$$

where V is the volume. Figure 6(d) shows the Grüneisen parameters of Sb_2Te and Sb_2Te_3 versus frequency. It is obviously seen that Sb_2Te possesses larger Grüneisen parameter (absolute value) than Sb_2Te_3. The mean values of Grüneisen parameters are 2.36 and 1.38 for Sb_2Te and Sb_2Te_3 along the out-of-plane direction (1.77 for Sb_2Te along in-plane direction), respectively. The above analysis shows that the low κ_L along out-of-plane direction of Sb_2Te is mainly caused by the lower group velocity and the stronger anharmonicity.

Table 2. Averaged lattice thermal conductivity of Sb_2Te and Sb_2Te_3.

Sb_2Te (W/mK)	Sb_2Te_3 (W/mK)			
0.9	4.1[59]	4.7[58]	5.0[61]	5.2[60]

To reveal the anharmonicity of Sb_2Te more clearly, we perform further analysis on the reduced atomic potential energy of Sb_2Te and Sb_2Te_3 with respect to displacement ratio, and the results are shown in Fig. 7(a). In the unit cell of each system, only one atom is moved away from the equilibrium position (along the out-of-plane direction), while the other atoms remain unchanged. We use a cubic function to fitting the reduced atomic potential energy. The absolute value of fitted cubic term of Sb_2Te (73.95) is larger than that of Sb_2Te_3 (9.11), which is similar to the Grüneisen parameters and also reveals the strong phonon anharmonicity in Sb_2Te. As is well-known, the electron localization function (ELF) uses the local influence information of Pauli repulsion to measure the localization degree of electrons in a solid, thus an image of lone-pair electrons can be directly given.[65] To further analyze the anharmonicity in Sb_2Te, the ELF is given in Fig. 7(b). It is found that there is electronic localization near the red spherical-like region around the Sb atom in Sb_2 bilayers of Sb_2Te, which is caused by the lone-pair electrons of the Sb atom. In the Sb_2 bilayer, one Sb atom and three Sb atoms form a triangular pyramid. The outermost electron configuration of Sb is $5s^25p^3$, in which three electrons form three groups of Sb–Sb covalent bonds with electrons of other surrounding Sb atoms and the other group of electrons become the lone-pair in this arrangement. In general, for materials containing lone-pair electrons, non-bonded electrons will interact with the valence electrons of the adjacent neighboring atoms, causing increased anharmonicity at limited temperature.[39] Therefore, it can be concluded that the stronger phonon anharmonicity in Sb_2Te is mainly due to the presence of lone-pair electrons.

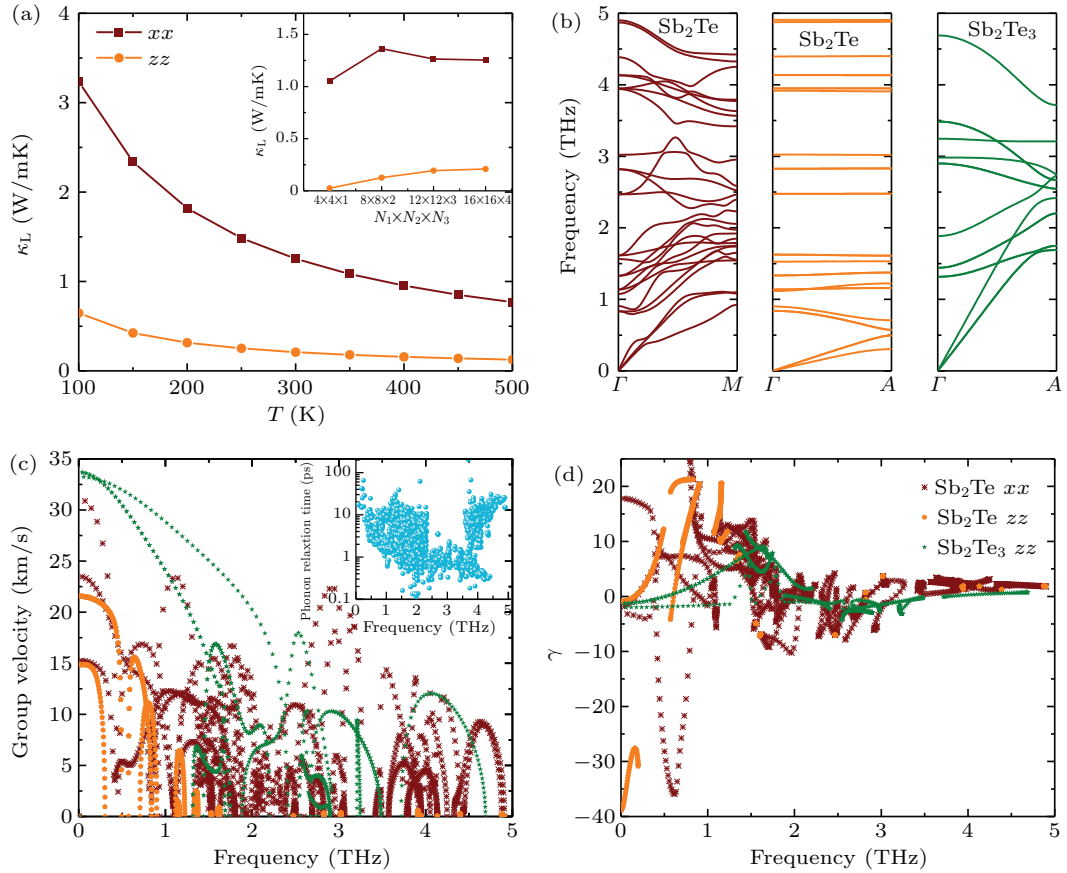


Fig. 6. (a) Lattice thermal conductivity (κ_L) of Sb_2Te along different directions as a function of temperature and q-grid (inset); (b) phonon dispersion curves of Sb_2Te and Sb_2Te_3 along the in-plane (Γ–M) and out-of-plane (Γ–A) directions; (c) phonon group velocity and (d) Grüneisen parameter of Sb_2Te and Sb_2Te_3 as a function of frequency along the in-plane (xx) and out-of-plane (zz) directions. The inset of in (c) is the phonon relaxation times of Sb_2Te.

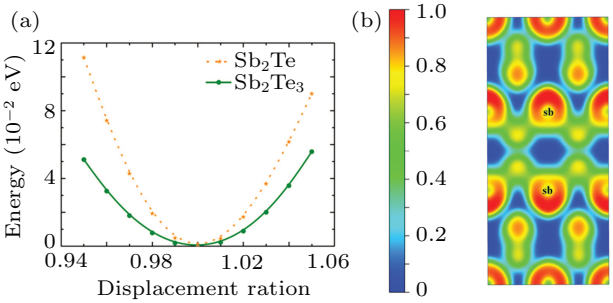


Fig. 7. (a) Potential energy change with respect to displacement of the atom from the equilibrium position. Displacement ratio ΔZ is defined as $\Delta Z = 1.0 + (Z - Z_0)/Z_0$, where Z and Z_0 represent the coordinates of shift and equilibrium positions, respectively. (b) Electron localization function (ELF) of Sb_2Te along the [100] direction within a $1 \times 2 \times 1$ supercell.

Based on the above results of electronic and phononic transport properties, one can evaluate the figure of merit, i.e., ZT. The calculated ZT values of Sb_2Te for both p- and n-types are shown in Fig. 8. The ZT of the n-type is larger than that of the p-type, which mainly stems from the anisotropic Seebeck coefficient and electric conductivity. The anisotropy that varies with the carrier concentration mainly depends on the complex competitive relationship between the transport coefficients. For example, at 400 K, the maximum ZT of n-type along the out-of-plane direction is larger than that along the in-plane direction. However, at 300 K, the peak value of ZT of n-type along the out-of-plane direction is smaller than that along the in-plane direction. It can be found that from Figs. 9(a) and 9(b) that both the power factor and total thermal conductivity along in-plane direction are larger than those along out-of-plane direction. According to the definition of ZT, the former is directly proportional to ZT and the latter is inversely proportional to ZT. The influence of anisotropy of power factor is mainly greater than that of thermal conductivity at 300 K. When the temperature is greater than 300K, the situation is just the opposite. As can be seen from Fig. 9(c), with the increase of temperature, ZT along the out-of-plane direction will always be greater than that in the in-plane direction. Because of the high Seebeck coefficient and relatively low κ_L, it is unsurprising to observe a quite promising value of ZT. At 300 K, the peak values of the ZT curves along the in-plane (out-of-plane) direction is about 0.60 (0.68) at a hole concentration of 4.72×10^{19} (3.32×10^{19}) cm^{-3}. Meanwhile, when the electron concentrations are 6.90×10^{19} and 1.19×10^{20} cm^{-3}, respectively, maximal ZT values of 1.46 and 1.38 can be achieved in the in-plane and out-of-plane directions. Even the electron relaxation time is reduced by half, as plotted in Fig. S1 in the supplementary material, the thermoelectric figure of merit ZT of monolayer Sb_2Te could still approach 0.39 (with p-type doping) and 1.08 (with n-type doping) along in-plane direction. These values are much larger than those of Sb_2Te_3 (0.13 along the in-plane direction and 0.23 along the out-of-plane direction) and even comparable to those of Bi_2Te_3.[46] Overall, our results indicate that Sb_2Te is a promising candidate for room-temperature TE materials.

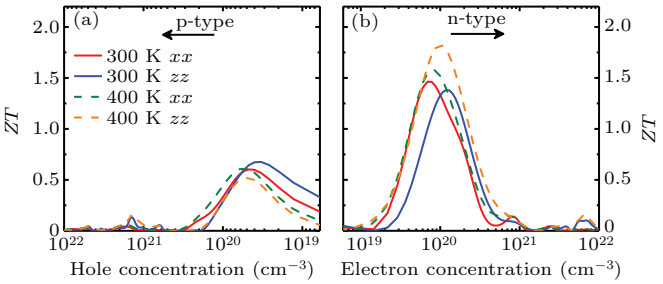


Fig. 8. Calculated figure of merit (ZT) of Sb_2Te as a function of carrier concentration [(a) holes and (b) electrons] along the in-plane (xx) and out-of-plane directions (zz) at 300 and 400 K.

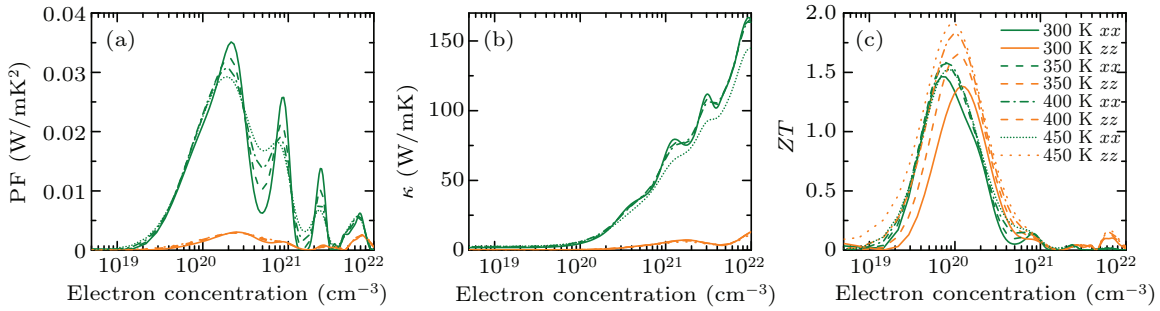


Fig. 9. (a) Power factor ($S^2\sigma$), (b) thermal conductivity ($\kappa = \kappa_{e+}\kappa_L$) and (c) ZT as a function of electron concentration along the in-plane (xx) and out-of-plane directions (zz) at different temperatures.

4. Conclusion

In summary, we have theoretically explored the electronic and phonon transport properties of Sb_2Te based on the first-principle calculations and Boltzmann transport theory. The results show that Sb_2Te possesses high Seebeck coefficients and low lattice thermal conductivity at room temperature. Since steeper DOS around CB, large Seebeck coefficients can approach 249.59 and 318.87 μV/K along the in-plane and out-of-plane directions for n-type Sb_2Te, respectively. Additionally, the unique SL structure, small phonon group velocity and strong anharmonicity of Sb_2Te lead to an ultralow lattice thermal conductivity of 1.25 (0.21) W/mK along the in-plane (out-of-plane) direction at 300 K. Further analysis shows that the small group velocity caused by the

flatter phonon spectrum is mainly due to the increase in interface scattering. The presence of lone pairs of electrons causes the strong anharmonicity. The ZT values of n-type Sb_2Te are as high as 1.46 and 1.38 at 300 K along the in-plane (at 6.90×10^{19} cm^{-3} electronic concentrations) and out-of-plane direction (at 1.19×10^{20} cm^{-3} electronic concentrations). Our work reveals the thermoelectric intrinsic mechanism of Sb_2Te, which will highlight the theoretical guidance for researchers who are interested in exploring new high-performance room temperature TE materials.

References

[1] Majumdar A 2004 *Science* **303** 777
[2] Snyder G J and Toberer E S 2008 *Nat. Mater.* **7** 105
[3] Zhang X and Zhao L D 2015 *J. Mater.* **1** 92
[4] Wang Z, Zhao L, Mak K F and Shan J 2017 *Nano Lett.* **17** 740
[5] Hansson J, Nilsson T M, Ye L and Liu J 2018 *Int. Mater. Rev.* **63** 22
[6] Takabatake T, Suekuni K, Nakayama T and Kaneshita E 2014 *Rev. Mod. Phys.* **86** 669
[7] Liu H, Shi X, Xu F, Zhang L, Zhang W, Chen L, Li Q, Uher C, Day T and Snyder G J 2012 *Nat. Mater.* **11** 422
[8] Jia P Z, Zeng Y J, Wu D, Pan H, Cao X H, Zhou W X, Xie Z X, Zhang J X and Chen K Q 2019 *J. Phys.: Condens. Matter* **32** 055302
[9] Cupo A and Meunier V 2017 *J. Phys.: Condens. Matter* **29** 283001
[10] Landry E S, Hussein M I and McGaughey A J H 2008 *Phys. Rev. B* **77** 184302
[11] Chen G, Dresselhaus M S, Dresselhaus G, Fleurial J P and Cailla T 2003 *Int. Mater. Rev.* **48** 45
[12] Boettner H, Chen G and Venkatasubramanian R 2006 *MRS Bull.* **31** 211
[13] Capinski W S and Maris H J 1996 *Physica B* **219–220** 699
[14] Capinski W S, Maris H J, Ruf T, Cardona M, Ploog K and Katzer D S 1999 *Phys. Rev. B* **59** 8105
[15] Lee S M, Cahill D G and Venkatasubramanian R 1997 *Appl. Phys. Lett.* **70** 2957
[16] Venkatasubramanian R 2000 *Phys. Rev. B* **61** 3091
[17] Venkatasubramanian R, Siivola E, Colpitts T and O'Quinn B 2001 *Nature* **413** 597
[18] Chong T C, Shi L P, Zhao R, Tan P K, Li J M, Lee H K, Miao X S, Du A Y and Tung C H 2006 *Appl. Phys. Lett.* **88** 122114
[19] Tong H, Miao X S, Cheng X M, Wang H, Zhang L, Sun J J, Tong F and Wang J H 2011 *Appl. Phys. Lett.* **98** 101904
[20] Long P, Tong H and Miao X 2012 *Appl. Phys. Express* **5** 031201
[21] Luo H, Gibson Q, Krizan J and Cava R J 2014 *J. Phys.: Condens. Matter* **26** 206002
[22] Agafonov V, Rodier N, Céolin R, Bellissent R, Bergman C and Gaspard J 1991 *Acta Crystallog. Sec. C* **47** 1141
[23] Zhu M, Wu L, Rao F, Song Z, Li X, Peng C, Zhou X, Ren K, Yao D and Feng S 2011 *J. Alloys Compd.* **509** 10105
[24] Darmawikarta K, Lee B S, Shelby R M, Raoux S, Bishop S G and Abelson J R 2013 *J. Appl. Phys.* **114** 034904
[25] Zheng Y, Cheng Y, Zhu M, Ji X, Wang Q, Song S, Song Z, Liu W and Feng S 2016 *Appl. Phys. Lett.* **108** 052107
[26] Liu G, Wu L, Zhu M, Song Z, Rao F, Song S and Cheng Y 2017 *Solid-State Electron.* **135** 31
[27] Meng Y, Ji X, Han P, Song Z, Zhou W, Guo W, Qian B and Wu L 2015 *ECS Solid State Lett.* **4** P4
[28] Guo S, Xu L, Zhang J, Hu Z, Li T, Wu L, Song Z and Chu J 2016 *Sci. Rep.* **6** 33639
[29] Blöchl P E 1994 *Phys. Rev. B* **50** 17953
[30] Kresse G and Joubert D 1999 *Phys. Rev. B* **59** 1758
[31] Hafner J 2008 *J. Comput. Chem.* **29** 2044
[32] Perdew J P, Burke K and Ernzerhof M 1996 *Phys. Rev. Lett.* **77** 3865
[33] Klimeš J, Bowler D R and Michaelides A 2011 *Phys. Rev. B* **83** 195131
[34] Heyd J and Scuseria G E 2004 *J. Chem. Phys.* **121** 1187
[35] Heyd J, Peralta J E, Scuseria G E and Martin R L 2005 *J. Chem. Phys.* **123** 174101
[36] Madsen G K H and Singh D J 2006 *Comput. Phys. Commun.* **175** 67
[37] Fan D D, Liu H J, Cheng L, Jiang P H, Shi J and Tang X F 2014 *Appl. Phys. Lett.* **105** 133113
[38] Sun P P, Bai L, Kripalani D R and Zhou K 2019 *npj Comput. Mater.* **5** 9
[39] Zhu X L, Liu P F, Zhang J, Zhang P, Zhou W X, Xie G and Wang B T 2019 *Nanoscale* **11** 19923
[40] Zhu X L, Hou C H, Zhang P, Liu P F, Xie G and Wang B T 2020 *J. Phys. Chem. C* **124** 1812
[41] Zhu X L, Yang H, Zhou W X, Wang B, Xu N and Xie G 2020 *ACS Appl. Mater. Interfaces* **12** 36102
[42] Xing G, Sun J, Li Y, Fan X, Zheng W and Singh D J 2017 *Phys. Rev. Mater.* **1** 065405
[43] Li W, Carrete J, Katcho N A and Mingo N 2014 *Comput. Phys. Commun.* **185** 1747
[44] Togo A and Tanaka I 2015 *Scr. Mater.* **108** 1
[45] Li W, Lindsay L, Broido D, Stewart D A and Mingo N 2012 *Phys. Rev. B* **86** 174307
[46] Hinsche N F, Yavorsky B Y, Mertig I and Zahn P 2011 *Phys. Rev. B* **84** 165214
[47] Pei Y, Shi X, LaLonde A, Wang H, Chen L and Snyder G J 2011 *Nature* **473** 66
[48] Xi J, Long M, Tang L, Wang D and Shuai Z 2012 *Nanoscale* **4** 4348
[49] Van Der Zande A M, Huang P Y, Chenet D A, Berkelbach T C, You Y, Lee G H, Heinz T F, Reichman D R, Muller D A and Hone J C J N m 2013 *Nat. Mater.* **12** 554
[50] Cai Y, Zhang G and Zhang Y W 2014 *J. Am. Chem. Soc.* **136** 6269
[51] Jonson M and Mahan G D 1980 *Phys. Rev. B* **21** 4223
[52] Sales B C, Mandrus D, Chakoumakos B C, Keppens V and Thompson J R 1997 *Phys. Rev. B* **56** 15081
[53] Dyck J S, Chen W, Uher C, Drašar Č and Lošt'ák P 2002 *Phys. Rev. B* **66** 125206
[54] Wu Y Y, Zhu X L, Yang H Y, Wang Z G, Li Y H and Wang B T 2020 *Chin. Phys B* **29** 087202
[55] Xie G, Ding D and Zhang G 2018 *Adv. Phys. X* **3** 1480417
[56] Xie G, Ju Z, Zhou K, Wei X, Guo Z, Cai Y and Zhang G 2018 *npj Comput. Mater.* **4** 21
[57] Zhang P, Ouyang T, Tang C, He C, Li J, Zhang C, Hu M and Zhong J 2018 *Modelling and Simulation in Materials Science and Engineering* **26** 085006
[58] Wang W, Yan X, Poudel B, Ma Y, Hao Q, Yang J, Chen G and Ren Z 2008 *J. Nanosci. Nanotechnol.* **8** 452
[59] Dhar S N and Desai C F 2010 *Philos. Mag. Lett.* **82** 581
[60] Jacquot A, Farag N, Jaegle M, Bobeth M, Schmidt J, Ebling D and Böttner H 2010 *J. Electron. Mater.* **39** 1861
[61] Heremans J P, Cava R J and Samarth N 2017 *Nat. Rev. Mater.* **2** 17049
[62] Chen G and Neagu M 1997 *Appl. Phys. Lett.* **71** 2761
[63] G C 1998 *Phys. Rev. B* **57** 14958
[64] Tamura S I, Tanaka Y and Maris H J 1999 *Phys. Rev. B* **60** 2627
[65] Wang H, Qin G, Qin Z, Li G, Wang Q and Hu M 2018 *J. Phys. Chem. Lett.* **9** 2474